SCIENTIFIC REPORTS
nature research

OPEN

Hybrid two-mode squeezing of microwave and optical fields using optically pumped graphene layers

Montasir Qasymeh[1]✉ & Hichem Eleuch[2,3]

A measurable quadrature of a squeezed quantum state manifests a small uncertainty below the Heisenberg limit. This phenomenon has the potential to enable several extraordinary applications in quantum information, metrology and sensing, and other fields. Several techniques have been implemented to realize squeezed electromagnetic states, including microwave fields and optical fields. However, hybrid squeezed modes (that incorporate both microwave and optical fields) have not yet been proposed despite their vital functionality to combine the two worlds of quantum superconducting systems and photonics systems. In this work, for the first time, we propose a novel approach to achieve two-mode squeezing of microwave and optical fields using graphene based structure. The proposed scheme includes a graphene layered structure that is driven by a quantum microwave voltage and subjected to two optical fields of distinct frequencies. By setting the optical frequency spacing equal to the microwave frequency, an interaction occurs between the optical and microwave fields through electrical modulation of the graphene conductivity. We show that significant hybrid two-mode squeezing, that includes one microwave field and one optical field, can be achieved. Furthermore, the microwave frequency can be tuned over a vast range by modifying the operation parameters.

Microwave fields with squeezed states hold promises for realizing quantum communication systems[1] and fault-tolerant quantum computation[2] and for connecting quantum computers[3]. Additionally, such fields can enable many unprecedented applications, including quantum radar and navigation[4–6], quantum metrology[7], and weak classical signal detection[8]. Moreover, squeezed optical fields, which are equally functional to all above applications, are also used in gravitational wave detection[9], laser system stabilization[10], achieving accurate gyroscope systems[11], detecting single-molecule[12], and to realize quantum memory[13], just to mention few.

Mainly three configurations have been successfully implemented to achieved squeezed microwave fields. These are Josephson parametric amplifiers (JPAs)[14], superconductor resonators[15], and electromechanical resonators[16]. Microwave squeezing with JPAs is based on using the JPA nonlinear response to form nonlinear resonators[17]. A typical squeezing gain of approximately 10 dB over a few MHz bandwidth is achieved[18]. Extended designs including Josephson traveling wave amplifiers with a squeezing gain of 20 dB and a bandwidth up to a few GHz have also been reported[19]. However, phase matching is required[20]. In contrast, microwave squeezing with gain up to 8 dB is achieved using superconductor resonators by implementing dissipation engineering to a coupled microwave field[21,22]. Squeezing with electromechanical resonators has been reported by using the radiation pressure force of the interacting field[23]. Squeezing gains up to 8 dB over a few tens of MHz are typically achieved[24]. However, the operation is temperature dependent, and the performance degrades for higher microwave frequencies. Similarly, squeezed optical fields have been achieved with gain of more than 15 dB either by implementing optical nonlinear materials[25] or by incorporating optomechanical systems[26]. Optical squeezing utilizing nonlinear optical materials are conducted by means of wave mixing or parametric down-conversion[27], while optical squeezing utilizing optomechanical systems is realized by coupling the light photons to mechanical motion via incorporating mechanical resonator in an optical cavity[28].

[1]Electrical and Computer Engineering Department, Abu Dhabi University, Abu Dhabi, UAE. [2]Department of Applied Physics and Astronomy, University of Sharjah, Sharjah, UAE. [3]Institute for Quantum Science and Engineering, Texas AM University, Texas, USA. ✉email: montasir.qasymeh@adu.ac.ae

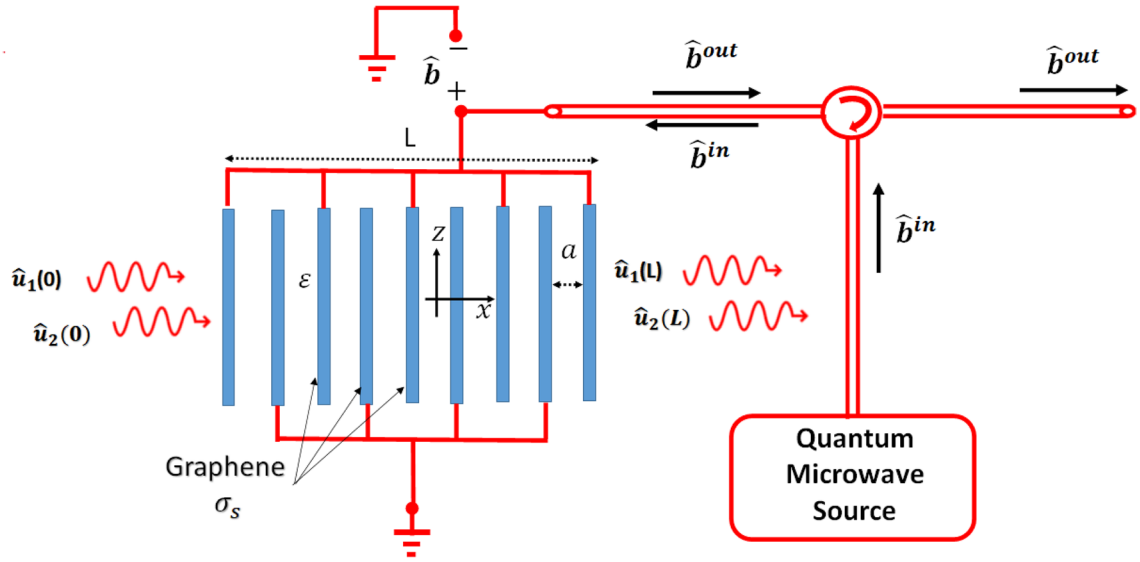

Figure 1. Proposed graphene layered structure driven by a $\hat{b}$ microwave field and subject to $\hat{u}_1$ and $\hat{u}_2$ optical input fields.

In this work, we propose a novel scheme for hybrid two-mode squeezing of microwave and optical fields. The proposed scheme utilizes an electro-optic interaction obtained by electrically modulating the graphene conductivity. A microwave field (of frequency ω_m) drives the graphene layers. The graphene layers are subject to two optical fields with frequencies ω_1 and ω_2. The interaction between the microwave and optical fields is enabled by setting $\omega_1 - \omega_2 = \omega_m$. A quantum mechanics model is developed to describe the electro-optic interaction. The microwave and optical fields are determined in the steady state, in which the time rate changes of their averages are zero. The operator fluctuations are evaluated by calculating the squeezing spectrum. The microwave field is conceived as the signal, while the optical fields at ω_1 and ω_2 are considered as the pump and the idler, respectively. We show that hybrid two-mode squeezing—that includes microwave field (i.e., the signal) and optical field (i.e., the idler)—can be achieved with a peak squeezing gain of 36 dB over about 2 MHz fluctuation spectrum bandwidth. Furthermore, the squeezed microwave frequency can be tuned over a wide range by modifying the optical frequency spacing. Achieving a hybrid two-mode squeezing paves the way towards merging the superconducting quantum systems with photonics systems. It then ultimately leads to hybrid systems that leverage the advantages of both[29]. Furthermore, the advantages of our proposed squeezing scheme include its simple structure (with no phase matching or SQUID insertion required), moderate cryogenic operation temperature, and tunability over a vast microwave frequency range.

Results

Model. The proposed structure is composed of periodic graphene layers connected in an interdigital configuration and electrically driven by a transmission line, as shown in Fig. 1. The graphene layers have periodicity a and cross-sectional area A_r and are filled with a dielectric material of permittivity ε. The transmission line is used to electrically drive the graphene layers by a microwave $\hat{b}^{in}$ voltage operator of frequency ω_m. The transmission line is connected to every other graphene layer, while the middling graphene layers are grounded. Thus, the graphene layers can be considered as $(N-1)$ identical shunted capacitors, each of $C = \frac{\varepsilon\varepsilon_0}{a}$ per unit area capacitance[30]. Electrically, the graphene layers are equivalent to a capacitor of $C_T = (N-1)C$ per unit area capacitance, as shown in Fig. 2. Here, N is the number of graphene layers. In this work, the intrinsic impedance of the transmission line is considered to be much smaller than the capacitor impedance of the graphene layers, yielding total microwave reflection. Thus, the total microwave voltage driving the graphene layers is given by $\hat{b} = \hat{b}^{out} + \hat{b}^{in}$, where $\hat{b}^{out}$ and $\hat{b}^{in}$ are the reflected and incident microwave voltage operators, respectively.

Additionally, two optical fields $\hat{u}_1$ and $\hat{u}_2$ are launched normally to the graphene layers. The optical fields have distinct frequencies ω_1 and ω_2, respectively. By setting $\omega_1 - \omega_2 = \omega_m$, interaction of the optical and microwave operators is enabled by electrically controlling the graphene conductivity. Optically, the graphene layers can be described by the concept of the effective permittivity, which can be obtained from the dispersion relation $\cos(a\beta) = \cos\left(a\sqrt{\varepsilon}\frac{\omega}{c}\right) - i\frac{Z_0}{2\sqrt{\varepsilon}}\sin\left(a\sqrt{\varepsilon}\frac{\omega}{c}\right)\sigma_s$[31]. Here, β represents the optical propagation constant, $Z_0 = 377\ \Omega$ is the free space impedance, c denotes the speed of light in vacuum, $\sigma_s = \frac{iq^2}{4\pi\hbar}ln\left(\frac{2\mu_c - (\frac{\omega}{2\pi} + i\tau^{-1})\hbar}{2\mu_c + (\frac{\omega}{2\pi} + i\tau^{-1})\hbar}\right) + \frac{iq^2K_BT}{\pi\hbar^2(\frac{\omega}{2\pi} + i\tau^{-1})}\left(\frac{\mu_c}{K_BT} + 2ln\left(e^{-\frac{\mu_c}{K_BT}} + 1\right)\right)$ is the graphene conductivity, q represents the electron charge, $\hbar$ denotes Planck's constant, τ is the scattering relaxation time in graphene, K_B represents the Boltzmann constant, and T is the temperature.

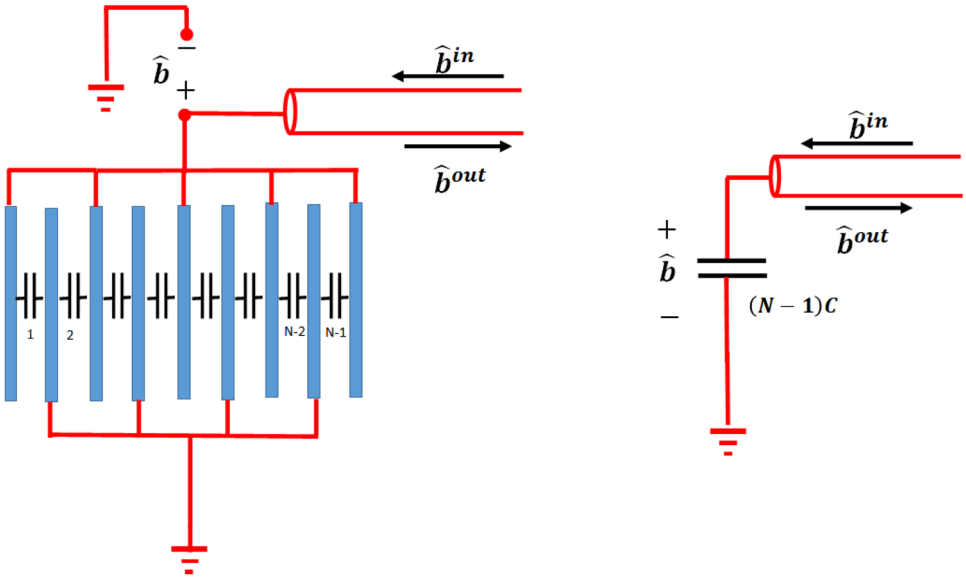

Figure 2. Equivalent electrical circuit of the graphene layer structure.

Following a similar perturbation approach to that developed in our previous work (see Supplementary Material 1)[30,32], the quantum Hamiltonian $\hat{\mathcal{H}} = \hat{\mathcal{H}}_0 + \hat{\mathcal{H}}_1$ is given by:

$$\hat{\mathcal{H}}_0 = \hbar\omega_m \hat{b}^\dagger \hat{b} + \sum_{j=1}^{2} \hbar\omega_j \hat{u}_j^\dagger \hat{u}_j, \tag{1}$$

$$\hat{\mathcal{H}}_1 = \hbar g \hat{u}_2^\dagger \hat{b}^\dagger \hat{u}_1 + \hbar g^* \hat{u}_1^\dagger \hat{b} \hat{u}_2 + h.c., \tag{2}$$

where $\hat{\mathcal{H}}_0$ and $\hat{\mathcal{H}}_1$ are the free and interaction Hamiltonians, respectively, $g = \varepsilon'' \sqrt{\frac{\omega_1\omega_2}{\varepsilon_1'\varepsilon_2'}} \sqrt{\frac{\hbar\omega_m}{CA_r}} sinc\left(\frac{\beta_1-\beta_2}{2}L\right) e^{i\frac{\beta_1-\beta_2}{2}L}$ is the coupling rate, *h.c.* denotes the Hermitian conjugate, $\varepsilon' = \frac{\beta^2}{k_0^2}$ is the effective permittivity, $\varepsilon'' = 2\frac{\beta\beta''}{k_0^2}$ represents the permittivity perturbation, $\beta'' = i\frac{Z_0}{2d\sqrt{\varepsilon}} \frac{\sin\left(d\frac{2\pi f\sqrt{\varepsilon}}{c}\right)}{\sin(d\beta)} \sigma_s''$ is the propagation constant perturbation, $\sigma_s'' = \frac{iq^2}{\pi\hbar} \frac{(f+i\tau^{-1})\hbar}{4(\mu_c)^2-(f+i\tau^{-1})^2\hbar^2} \mu_c'' + \frac{iq^2K_BT}{\pi\hbar^2(f+i\tau^{-1})} tanh\left(\frac{\mu_c}{2K_BT}\right) \frac{\mu_c''}{K_BT}$ represents the graphene conductivity perturbation, $\mu_c = \hbar V_f \sqrt{\pi n_0}$ denotes the graphene chemical potential, $\mu_c'' = \hbar V_f \frac{C_T}{q\sqrt{\pi n_0}}$ is the chemical potential perturbation, and n_0 represents the electron density. The equations of motion can obtained by substituting the Hamiltonian into the Heisenberg equation of motion, that is, $\frac{\partial\hat{o}}{\partial t} = \frac{i}{\hbar}[\hat{\mathcal{H}}, \hat{o}]$. Losses can be taken in to account by incorporating the decay coefficients in the equations of motion. The optical decay rate includes the mode attenuation and layers transmittance, while the microwave field decay rate can be derived from electrical dissipation[30]. Importantly, according to the fluctuation-dissipation theorem, the Langevin forces (which represent the noise in the microwave and optical fields as the feed-back of the environment to the system) need to be included. Consequently, by implementing the standard rotation approximation, the equations of motion are given by:

$$\frac{\partial\hat{b}}{\partial t} = -\frac{\Gamma_m}{2}\hat{b} - ig(\hat{u}_1 + \alpha_1)\hat{u}_2^\dagger + \sqrt{\Gamma_m}\hat{n}_m, \tag{3}$$

$$\frac{\partial\hat{u}_1}{\partial t} = -\frac{\Gamma_1}{2}\hat{u}_1 - ig^*\hat{b}\hat{u}_2 + \sqrt{\Gamma_1}\hat{n}_1, \tag{4}$$

$$\frac{\partial\alpha_1}{\partial t} = -\frac{\Gamma_1}{2}\alpha_1, \tag{5}$$

$$\frac{\partial\hat{u}_2}{\partial t} = -\frac{\Gamma_2}{2}\hat{u}_2 - ig(\hat{u}_1 + \alpha_1)\hat{b}^\dagger + \sqrt{\Gamma_2}\hat{n}_2, \tag{6}$$

where α_1 is the classical component of the optical mode at frequency ω_1, $\Gamma_j = 2v_g Im(\beta_j) + \frac{v_g}{a} ln(\frac{1}{T_0^2})$ and $\Gamma_m = -\frac{2}{t_0} ln\left(1 - \frac{vt_0}{2qR_g}\right)$ are the optical and microwave decay coefficients, respectively, $\hat{n}_j$ denotes the quantum

Langevin noise operator, T_0 indicates the medium transmittance (calculated using the transfer matrix method[33]), t_0 is the time of flight over a single layer block, $R_g = Re(\frac{1}{\sigma_s})$, and $\nu = \left(\frac{\hbar\omega_m}{C_T A_r}\right)^{\frac{1}{2}} \hat{b}$ describes the classical counterpart of the quantum microwave annihilation operator. The quantum Langevin noise operator obeys the relations $[\hat{n}_j(t_1), \hat{n}_j(t_2)^\dagger] = \delta(t_1 - t_2)$ and $\langle n(t_1)^\dagger n(t_2)\rangle = \frac{1}{exp(\hbar\omega/k_B T)-1}\delta(t_1 - t_2)$. We remark here that the optical mode at frequency ω_1 is composed of quantum component and classical component. This is similar to having a strong pump component and weak field component. Analytically, this is taken into account by substituted $\hat{u}_1 + \alpha_1$ instead of $\hat{u}_1$ in the Heisenberg equation to achieve Eqs. (3)–(6). The classical component α_1 undertakes the role of the optical pumping.

By expressing the interacting operators in terms of their averages and fluctuations, i.e., $\hat{o} = \langle\hat{o}\rangle + \delta\hat{o}$, and then substituting them into the equations of motion in Eqs. (3)–(6), we obtain a set of rate equations for the operator averages and another set for the fluctuations[23]. The rate equations for the averages are given by:

$$\frac{\partial\langle\hat{b}\rangle}{\partial t} = -\frac{\Gamma_m}{2}\langle\hat{b}\rangle - ig\langle\hat{u}_1\rangle\langle\hat{u}_2^\dagger\rangle - ig\alpha_1\langle\hat{u}_2^\dagger\rangle, \tag{7}$$

$$\frac{\partial\langle\hat{u}_1\rangle}{\partial t} = -\frac{\Gamma_1}{2}\langle\hat{u}_1\rangle - ig^*\langle\hat{b}\rangle\langle\hat{u}_2\rangle, \tag{8}$$

$$\frac{\partial\langle\hat{u}_2\rangle}{\partial t} = -\frac{\Gamma_2}{2}\langle\hat{u}_2\rangle - ig\langle\hat{u}_1\rangle\langle\hat{b}^\dagger\rangle - ig\alpha_1\langle\hat{b}^\dagger\rangle. \tag{9}$$

It is worth mentioning that the average $\langle\hat{u}_1\rangle$ and α_1 are essentially different. The average $\langle\hat{u}_1\rangle$ is time dependent and governed by the equation of motion (8). In contrary, α_1 is an intensive classical quantity that is independent of time and subject only to dissipation. Our calculations show that $\langle\hat{u}_1\rangle$ tends to zero value at steady state for large α_1 value. The rate equations for the fluctuations are given by:

$$\frac{\partial\delta\hat{b}}{\partial t} = -\frac{\Gamma_m}{2}\delta\hat{b} - ig\langle\hat{u}_2^\dagger\rangle\delta\hat{u}_1 - ig\left(\alpha_1 + \langle\hat{u}_1\rangle\right)\delta\hat{u}_2^\dagger + \sqrt{\Gamma_m}\hat{n}_m, \tag{10}$$

$$\frac{\partial\delta\hat{u}_1}{\partial t} = -\frac{\Gamma_1}{2}\delta\hat{u}_1 - ig^*\langle\hat{u}_2\rangle\delta\hat{b} - ig^*\langle\hat{b}\rangle\delta\hat{u}_2 + \sqrt{\Gamma_1}\hat{n}_1, \tag{11}$$

$$\frac{\partial\delta\hat{u}_2}{\partial t} = -\frac{\Gamma_2}{2}\delta\hat{u}_2 - ig\langle\hat{b}^\dagger\rangle\delta\hat{u}_1 - ig\left(\alpha_1 + \langle\hat{u}_1\rangle\right)\delta\hat{b}^\dagger + \sqrt{\Gamma_2}\hat{n}_2. \tag{12}$$

The averages can be solved in the steady state for a given decay coefficient, i.e., Γ_j, and classical field component, i.e., α_1. Thus, the fluctuations, i.e., $\delta\hat{o}$, can be solved in the frequency domain (as shown in "Methods" section).

According to the incident-reflected relation in a transmission line, $\hat{b} = \hat{b}^{out} + \hat{b}^{in}$ for the case of total reflection. It then follows that the microwave output fluctuation is given by[34]:

$$\delta\hat{b} = \delta\hat{b}^{out} + \hat{n}_m, \tag{13}$$

The optical output fluctuations $\delta\hat{u}_2^{out}$ and $\delta\hat{b}$ can be evaluated by solving Eqs. (7)–(12). The squeezing of the hybrid two-modes can be quantified by calculating its fluctuation correlation. The spectrum of this fluctuation correlation (named the squeezing spectrum) is given by:

$$S_X(\omega) = \left\langle\delta\hat{X}_{out}(\omega)\delta\hat{X}_{out}(\omega)\right\rangle, \tag{14}$$

where $\delta\hat{X}_{out}(\omega) = \frac{1}{\sqrt{2}}\left(\delta\hat{b}^{out}(\omega) + \delta\hat{u}_2^{out}(\omega) + \delta\hat{b}^{out^\dagger}(\omega) + \delta\hat{u}_2^{out^\dagger}(\omega)\right)$[35]. Here, $\delta\hat{o}(\omega) = \mathcal{F}(\delta\hat{o}(t)) = \int_{-\infty}^{+\infty}\delta\hat{o}(t)e^{-i\omega t}\partial t$ is Fourier transform.

The squeezing spectrum is less than unity for two-mode squeezed quadrature[36,37].

Numerical estimations. In this section, numerical estimations are presented to study the viability of the proposed scheme. As detailed in Eq. (26), the squeezing spectrum is dependent on g (the coupling rate) and on Γ_1, Γ_2, and Γ_m (the decay coefficients). Our numerical simulations show that squeezing is achieved for specific combination of decay coefficients and coupling rate. Upon setting $a = \frac{\pi c}{2\omega_1\sqrt{\varepsilon}}$, Γ_1 and Γ_2 slightly change with the microwave frequency (as the optical fields are off-resonant with the layered graphene medium). Thus, under this condition, squeezing can be extended to over a larger microwave frequency range by controlling the coupling rate against the microwave frequency. The coupling rate can be electrically modified by disturbing the effective electron density of graphene with a DC bias. Hereby, wideband microwave squeezing is achieved.

In the following simulations, we consider a cryogenic temperature $T = 3$ mK and a silicon filling material with $\varepsilon = (3.5)^2$.

First, we evaluate the coupling rate versus different graphene design parameters. In Fig. 3, the coupling rate is evaluated versus the graphene electron density. Several medium lengths are considered. The coupling rate can

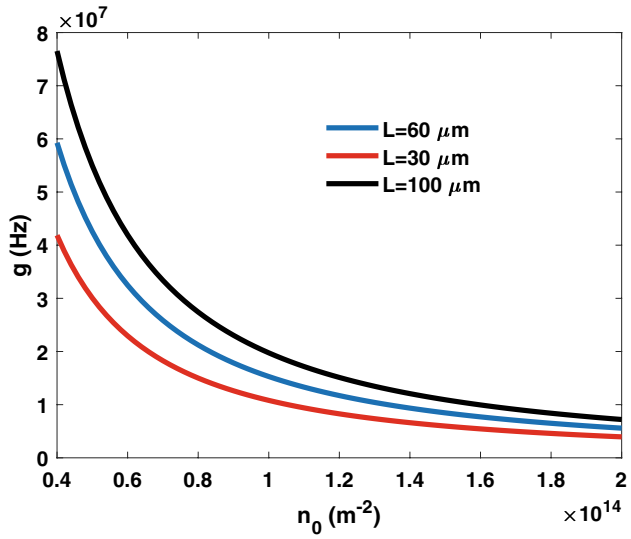

Figure 3. Coupling rate g versus graphene electron density. Several medium lengths are considered.

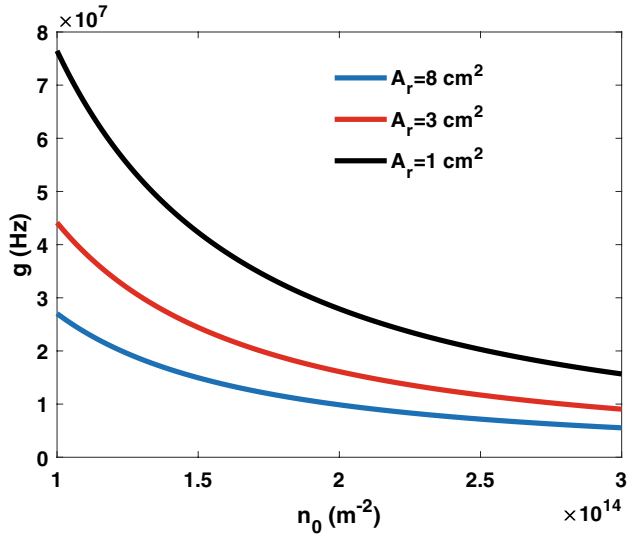

Figure 4. Coupling rate g versus graphene electron density. Different areas of the graphene layers are considered.

be set over a wide range by controlling the electron density and the medium length (i.e., the number of layers). Moreover, in Fig. 4, the conversion rate versus the electron density is displayed considering different graphene cross-sectional areas. Figures 3 and 4 demonstrate the feasibility of controlling the coupling rate by altering the graphene layer properties.

Upon finding the average values in the steady state, the squeezing spectrum can be evaluated. In Fig. 5, the squeezed spectrum S_X and squeezing gain $\left(\text{defined by } G_X = -10log_{10}[S_X]\right)$ of the output two-mode quadrature are shown for $\frac{\omega_m}{2\pi} = 10$ GHz. Here, $g = 20.24 \times 10^6$ Hz, and $\alpha_1 = 708$. The averages in the steady state are $\left\langle \hat{b} \right\rangle = 200$, $\left\langle \hat{u}_1 \right\rangle = 0$, and $\left\langle \hat{u}_2 \right\rangle = 7$. The optical decay coefficients calculated from the dispersion relation are $\Gamma_1 = \Gamma_2 = 8 \times 10^{11}$ Hz, and the microwave decay coefficient is $\Gamma_m = 1.02 \times 10^9$ Hz. These values were defined by carrying out significant numerical investigations. As seen, squeezing with significant gain is achieved over a bandwidth of almost 2 MHz with a peak of approximately 37 dB at $\omega = 0$. Here, ω is the frequency spectrum of the fluctuations.

Our simulations show that by setting $a = \frac{\pi c}{2\omega\sqrt{\varepsilon}} = 0.11$ μm, the decay coefficients change very slightly over the 10–100 GHz microwave frequency range. However, the coupling rate is function of the microwave frequency. Nonetheless, the coupling rate can be controlled by modifying the electron density of the graphene layers. It then follows squeezing can be extended against the microwave frequency range for proper combinations of ω_m and effective electron density. For instance, if the coupling rate is constant (against the microwave frequency) at

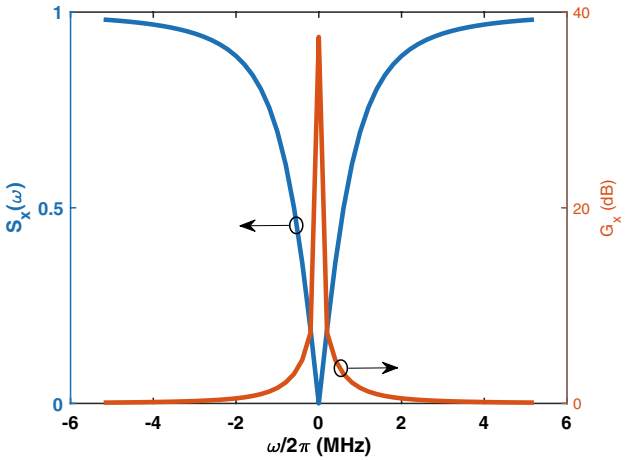

Figure 5. Squeezing spectrum $S_x(\omega)$ and squeezing gain G_X of the output two-mode quadrature. Here, $\frac{\omega_m}{2\pi} = 10$ GHz and $g = 20.24 \times 10^6$ Hz.

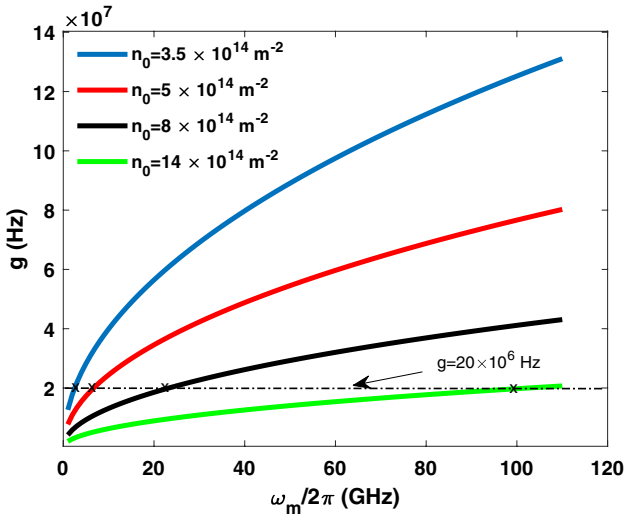

Figure 6. Coupling rate versus microwave frequency. Different electron densities are considered.

$g = 20.24 \times 10^6$ Hz, then the squeezing in Fig. 5 can be extended over the entire microwave frequency range from 10 to 100 GHz. In Fig. 6, the coupling rate is evaluated against the microwave frequency. Different electron densities are considered. As can be observed, the coupling rate can be maintained at $g = 20.24 \times 10^6$ Hz over the entire microwave frequency range by adjusting the electron density from 3.5×10^{14} m^{-2} to 14×10^{14} m^{-2}. The effective electron density can be modified by applying a DC electrical voltage as follows[38]:

$$n_{0_{eff}} = n_0 + 2\frac{C_T}{\pi q} V_{dc}, \tag{15}$$

where n_0 is the intrinsic electron density and V_{dc} is the DC bias voltage. The effective electron density is displayed in Fig. 7 against the DC bias voltage. As shown in Fig. 7, the effective electron density can be controlled over the required range, from 3.5×10^{14} m^{-2} to 14×10^{14} m^{-2}, by varying the DC bias from 0.1 to 0.6 m V for intrinsic electron density $n_0 = 1 \times 10^{14}$ m^{-2}.

Furthermore, we evaluate the squeezing gain against the temperature. In Fig. 8, the squeezing gain spectrum is evaluated for $T = 3$ mK, $T = 60$ mK, and $T = 90$ mK. The other parameters are the same as in Fig. 5. We observe that the squeezing gain can be maintained even up to moderate cryogenic temperatures. For example, for $T = 90$ mK, a squeezing gain can be obtained for an up to tens of kHz frequency bandwidth with a peak of 17 dB at $\omega = 0$. Our numerical investigations show that the graphene conductivity slightly changes with the temperature over this range. However, the squeezing limitations are attributed to the thermal noise contribution. This is a further advantage of the proposed scheme since operations at moderate cryogenic temperatures is practical requirement for quantum processors[39].

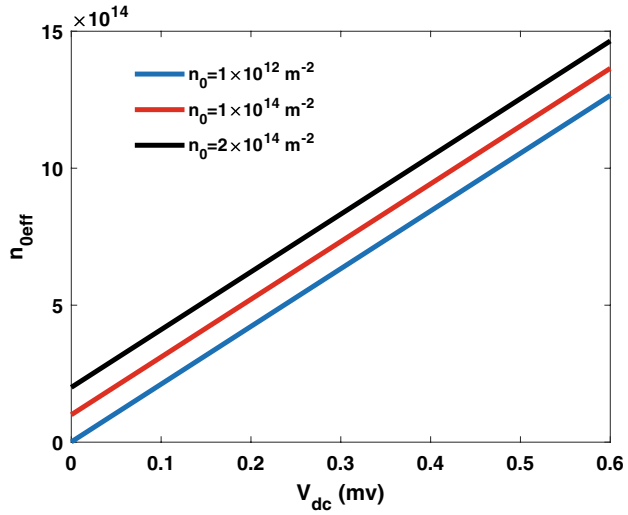

Figure 7. Effective electron density versus DC bias voltage. Different intrinsic electron densities are considered.

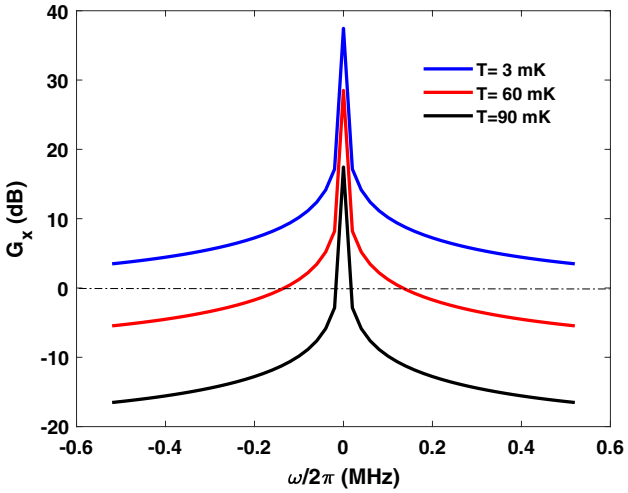

Figure 8. Squeezing gain spectrum. Different temperatures are considered.

Finally, we evaluate the optical pump power needed to achieve squeezing, given by $p = \frac{1}{2}\varepsilon_0\sqrt{\varepsilon'}A_r A_{\alpha_1}$, where $A_{\alpha_1} = \left(\frac{\hbar\omega_1}{\varepsilon_0\varepsilon' A_r L}\right)^{\frac{1}{2}}\alpha_1$ is the associated electric field intensity. For $\alpha_1 = 708$, the optical pump power is $p = 577$ mWThis is a moderate optical power value that can be supported by an off-the-shelf optical source.

Discussion

A novel modality for hybrid two-mode (microwave and optical) squeezing is proposed and thoroughly investigated utilizing graphene layered structure. The graphene layers are driven by a quantum electrical voltage and subjected to two optical fields. We have shown that by setting the frequency spacing between the optical fields equal to the microwave frequency and properly designing the classical component of the optical pump field, significant hybrid two-mode squeezing can be achieved. Inherited from the microwave photonics features, the proposed scheme exhibits several major advantages. First, the proposed scheme lays the ground to achieve hybrid quantum systems that leverage the advantages of both superconducting and photonic systems. Second, the structure is simple and requires only two optical fields with controlled frequency. Third, the microwave frequency can be simply tuned by controlling the optical frequency spacing and the coupling rate. Furthermore, the proposed scheme has a mild parametric temperature dependence, while the temperature limitations are attributed to the fluctuation–dissipation-type-induced thermal contribution. These properties open the way for practical implementation of squeezed hybrid modes in quantum microprocessors and other applications.

Methods. For simplification, we consider the following fields transformations:

$$\hat{u}_1 = \hat{U}_1,\ \hat{b} = i\hat{B},\ \hat{u}_2 = \hat{U}_2 e^{i\Theta},\ g = \mid g \mid e^{i\Theta}. \tag{16}$$

where Θ is a random phase angle. It then follows that the equations of motions are given by:

$$\frac{\partial \hat{B}}{\partial t} = -\frac{\Gamma_m}{2}\hat{B} - \mid g \mid \left(\hat{U}_1 + \alpha_1\right)\hat{U}_2^{\dagger} + \sqrt{\Gamma_m}\hat{n}_m, \tag{17}$$

$$\frac{\partial \hat{U}_1}{\partial t} = -\frac{\Gamma_1}{2}\hat{U}_1 + \mid g \mid \hat{B}\hat{U}_2 + \sqrt{\Gamma_1}\hat{n}_1, \tag{18}$$

$$\frac{\partial \alpha_1}{\partial t} = -\frac{\Gamma_1}{2}\alpha_1, \tag{19}$$

$$\frac{\partial \hat{U}_2}{\partial t} = -\frac{\Gamma_2}{2}\hat{U}_2 - \mid g \mid \left(\hat{U}_1 + \alpha_1\right)\hat{B}^{\dagger} + \sqrt{\Gamma_2}\hat{n}_2, \tag{20}$$

Similar to Eqs. (7)–(12), one can obtain rate equations for operators' averages and fluctuations.

On considering steady state (where $\frac{\partial\left\langle \hat{O}\right\rangle}{\partial t} = 0$), one gets 6 nonlinear equations of the 6 average operators: $\left\langle \hat{B}\right\rangle, \left\langle \hat{B}^{\dagger}\right\rangle, \left\langle \hat{U}_1\right\rangle, \left\langle \hat{U}_1^{\dagger}\right\rangle \left\langle \hat{U}_2\right\rangle$, and $\left\langle \hat{U}_2^{\dagger}\right\rangle$. On having several mathematical substitutions, these 6 equations can be simplified in form of the following three equations:

$$\begin{aligned} &\frac{\Gamma_m\Gamma_2}{\mid g \mid^2}\left[1 + \frac{4 \mid g \mid^2}{\Gamma_m\Gamma_1}\left\langle \hat{U}_2^{\dagger}\right\rangle\left\langle \hat{U}_2\right\rangle\right]^2 + 16\frac{\mid g \mid^2 \mid \alpha_1 \mid^2}{\Gamma_m\Gamma_1}\left\langle \hat{U}_2^{\dagger}\right\rangle\left\langle \hat{U}_2\right\rangle \\ &= 4 \mid \alpha_1 \mid^2 \left(1 + \frac{\mid g \mid^2}{\Gamma_m\Gamma_1}\left\langle \hat{U}_2^{\dagger}\right\rangle\left\langle \hat{U}_2\right\rangle\right), \end{aligned} \tag{21}$$

$$\left\langle \hat{B}\right\rangle = -2\alpha_1\frac{\mid g \mid}{\Gamma_m}\frac{\left\langle \hat{U}_2^{\dagger}\right\rangle}{1 + \frac{4\mid g\mid^2}{\Gamma_m\Gamma_1}\left\langle \hat{U}_2^{\dagger}\right\rangle\left\langle \hat{U}_2\right\rangle} \tag{22}$$

$$\left\langle \hat{U}_1\right\rangle = -4\alpha_1\frac{\mid g \mid^2}{\Gamma_m\Gamma_1}\frac{\left\langle \hat{U}_2^{\dagger}\right\rangle\left\langle \hat{U}_2\right\rangle}{1 + \frac{4\mid g\mid^2}{\Gamma_m\Gamma_1}\left\langle \hat{U}_2^{\dagger}\right\rangle\left\langle \hat{U}_2\right\rangle} \tag{23}$$

The nonlinear Eq. (21) can be solved numerically, for known decay coefficients and classical pump, giving $\left\langle \hat{U}_2\right\rangle$ value. Consequently, $\left\langle \hat{B}\right\rangle$ and $\left\langle \hat{U}_1\right\rangle$ can be calculated using Eqs. (22) and (23).

Second, by applying the Fourier transform to the equation set of the fluctuations, the solution of the operator fluctuation, in the frequency domain, is given by:

$$\boldsymbol{GR} = \boldsymbol{N}, \tag{24}$$

where

$$\boldsymbol{R} = \begin{pmatrix} \delta\hat{B}(\omega) \\ \delta\hat{B}^{\dagger}(\omega) \\ \delta\hat{U}_1(\omega) \\ \delta\hat{U}_1^{\dagger}(\omega) \\ \delta\hat{U}_2(\omega) \\ \delta\hat{U}_2^{\dagger}(\omega) \end{pmatrix}, \boldsymbol{N} = \begin{pmatrix} \sqrt{\Gamma_m}\hat{N}_m(\omega) \\ \sqrt{\Gamma_m}\hat{N}_m^{\dagger}(\omega) \\ \sqrt{\Gamma_1}\hat{N}_1(\omega) \\ \sqrt{\Gamma_1}\hat{N}_1^{\dagger}(\omega) \\ \sqrt{\Gamma_2}\hat{N}_2(\omega) \\ \sqrt{\Gamma_2}\hat{N}_2^{\dagger}(\omega) \end{pmatrix}, \tag{25}$$

$$\boldsymbol{G} = \begin{pmatrix} i\omega + \frac{\Gamma_m}{2} & 0 & \mid g \mid \left\langle \hat{U}_2^{\dagger}\right\rangle & 0 & 0 & \mid g \mid \alpha_1 + \mid g \mid \left\langle \hat{U}_1\right\rangle \\ 0 & -i\omega + \frac{\Gamma_m}{2} & 0 & \mid g \mid \left\langle \hat{U}_2\right\rangle & \mid g \mid \alpha_1^* + \mid g \mid \left\langle \hat{U}_1^{\dagger}\right\rangle & 0 \\ -\mid g \mid \left\langle \hat{U}_2\right\rangle & 0 & i\omega + \frac{\Gamma_1}{2} & 0 & -\mid g \mid \left\langle \hat{B}\right\rangle & 0 \\ 0 & -\mid g \mid \left\langle \hat{U}_2^{\dagger}\right\rangle & 0 & -i\omega + \frac{\Gamma_1}{2} & 0 & -\mid g \mid \left\langle \hat{B}^{\dagger}\right\rangle \\ 0 & \mid g \mid \alpha_1 + \mid g \mid \left\langle \hat{U}_1\right\rangle & \mid g \mid \left\langle \hat{B}^{\dagger}\right\rangle & 0 & i\omega + \frac{\Gamma_2}{2} & 0 \\ \mid g \mid \alpha_1^* + \mid g \mid \left\langle \hat{U}_1^{\dagger}\right\rangle & 0 & 0 & \mid g \mid \left\langle \hat{B}\right\rangle & 0 & -i\omega + \frac{\Gamma_2}{2} \end{pmatrix}. \tag{26}$$

For instance, the solution for the microwave annihilation operator is given by:

$$\begin{aligned}\delta\hat{B}(\omega) =& T_{1,1}\sqrt{\Gamma_m}\hat{N}_m(\omega) + T_{1,2}\sqrt{\Gamma_m}\hat{N}_m^{\dagger}(\omega) + T_{1,3}\sqrt{\Gamma_1}\hat{N}_1(\omega) \\ &+ T_{1,4}\sqrt{\Gamma_1}\hat{N}_1^{\dagger}(\omega) + T_{1,5} + \sqrt{\Gamma_2}\hat{N}_2(\omega) + T_{1,6}\sqrt{\Gamma_2}\hat{N}_2^{\dagger}(\omega),\end{aligned} \tag{27}$$

where $T_{l,k} = G^{-1}(l,k)$, $\langle N(\omega_1)^{\dagger}N(\omega_2)\rangle = \frac{2\pi}{exp(\hbar\omega/k_BT)-1}\delta(\omega_1+\omega_2)$, and $\langle N(\omega_1)N(\omega_2)^{\dagger}\rangle = 2\pi\ + \langle N(\omega_1)^{\dagger}N(\omega_2)\rangle$.

The solution for the other operators can be obtained in a similar way.

Data availability

The datasets generated during and/or analysed during the current study are available from the corresponding author on reasonable request.

Received: 23 June 2020; Accepted: 15 September 2020
Published online: 07 October 2020

References

1. Pogorzalek, S. *et al.* Finite-time quantum entanglement in propagating squeezed microwaves. *Sci. Rep.* **8**, 6416 (2017).
2. Tomita, K. F. A. & Okamoto, A. High-threshold fault-tolerant quantum computation with analog quantum error correction. *Phys. Rev. X* **8**, 021054 (2018).
3. Fedorov, K. *et al.* Secure quantum remote state preparation of squeezed microwave states. *Nat. Commun.* **10**, 2604 (2019).
4. Chang, C. W., Vadiraj, A. M., Bourassa, J., Balaji, B. & Wilson, C. M. Quantum-enhanced noise radar. *Appl. Phys. Lett.* **114**, 112601 (2019).
5. Rajan, D. L. S. & Balaji, B. Quantum two-mode squeezing radar and noise radar: Correlation coefficients for target detection. *IEEE Sens. J.* **20**, 5221–5228 (2020).
6. Wei, X. L. D. W. Q. M. H. Z. T. A navigation ranging scheme with true random eentangled microwave signals. *IEEE Photon. J.* **10**, 6101107 (2018).
7. Campagne-Ibarcq, P. *et al.* Magnetic resonance with squeezed microwaves. *Phys. Rev. X* **7**, 041011 (2017).
8. Palken, D. A. *et al.* Squeezed vacuum used to accelerate the search for a weak classical signal. *Phys. Rev. X* **9**, 021023 (2019).
9. Aasi, J. & Abadie, J. Z. Enhanced sensitivity of the ligo gravitational wave detector by using squeezed states of light. *Nat. Photon* **7**, 613–619 (2013).
10. Henning, V., Dennis, W., Moritz, M. & Benno, W. Laser power stabilization beyond the shot noise limit using squeezed light. *Phys. Rev. Lett.* **121**, 173601 (2018).
11. Fan, S. W. L. S. & Digonnet, M. J. F. Experimental observation of low noise and low drift in a laser-driven fiber optic gyroscope. *J. Lightw. Technol.* **31**, 2079–2085 (2013).
12. Mauranyapin, N. *et al.* Evanescent single-molecule biosensing with quantum-limited precision. *Nat. Photon* **11**, 477–481 (2017).
13. Jensen, K., Wasilewski, W. & Krauter, H. Quantum memory for entangled continuous-variable states. *Nat. Phys* **7**, 13–16 (2011).
14. Zhong, L. *et al.* Squeezing with a flux-driven josephson parametric amplifier. *New J. Phys.* **15**, 125013 (2013).
15. Zagoskin, A. *et al.* Controlled generation of squeezed states of microwave radiation in a superconducting resonant circuit. *Phys. Rev. Lett.* **101**, 253602 (2008).
16. Huo, W. & Long, G. Generation of squeezed states of nanomechanical resonator using three wave mixing. *Appl. Phys. Lett.* **92**, 133102 (2008).
17. Castellannos-Beltran, M. *et al.* Amplification and squeezing of quantum noise with a tunable josephson metamaterial. *Nat. Phys.* **4**, 929–931 (2008).
18. Gambetta, J. B. F. B. J. M. & Blais, A. Josephson-junction-embedded transmission-line resonators: From kerr medium to in-line transmon. *Phys. Rev. A* **86**, 013814 (2012).
19. OBrien, K. *et al.* A nearquantum-limited josephson traveling-wave parametric amplifier. *Science* **350**, 307–310 (2015).
20. Grimsmo, A. & Blais, A. Squeezing and quantum state engineering with josephson travelling wave amplifiers. *NPJ Quant. Inf.* **3**, 20 (2017).
21. Garca-Ripoll, J. *et al.* Inducing nonclassical lasing via periodic drivings in circuit quantum electrodynamics. *Appl. Phys. Lett.* **113**, 193601 (2014).
22. Xie, J., Ma, S., Ren, Y., Li, X. & Li, F. Dissipative generation of steady-state squeezing of superconducting resonators via parametric driving. *Phys. Rev. A* **101**, 012348 (2020).
23. Sete, E. & Eleuch, H. Strong squeezing and robust entanglement in cavity electromechanics. *Phys. Rev. A* **89**, 013841 (2014).
24. Sillanp, M. *et al.* Noiseless quantum measurement and squeezing of microwave fields utilizing mechanical vibrations. *Appl. Phys. Lett.* **118**, 103601 (2017).
25. Wu, L. A., Kimble, H. J., Hall, J. L. & Wu, H. Generation of squeezed states by parametric down conversion. *Appl. Phys. Lett.* **57**, 2520–2523 (1986).
26. Markus, A., Kippenberg, T. J. & Florian, M. Cavity optomechanics. *Rev. Mod. Phys.* **86**, 1391–1452 (2014).
27. Henning, V., Moritz, M., Karsten, D. & Roman, S. Detection of 15 db squeezed states of light and their application for the absolute calibration of photoelectric quantum efficiency. *Appl. Phys. Lett.* **117**, 110801 (2016).
28. Purdy, T. P. *et al.* Strong optomechanical squeezing of light. *Phys. Rev. X* **3**, 031012 (2013).
29. Qasymeh, M. & Eleuch, H. Entanglement of microwave and optical fields using electrical capacitor loaded with plasmonic graphene waveguide. *IEEE Photon. J.* **12**, 7500212 (2020).
30. Qasymeh, M. & Eleuch, H. Quantum microwave-to-optical conversion in electrically driven multilayer graphene. *Opt. Express* **27**, 5945–5960 (2019).
31. Qasymeh, M. Giant amplification of terahertz waves in a nonlinear graphene layered medium. *IEEE Photon. Tech Lett.* **30**, 35–38 (2018).
32. Qasymeh, M. & Eleuch, H. Graphenebased layered structure for quantum microwave signal upconversion to the optical domain. *Opt. Quant. Electron.* **52**, 80 (2020).
33. Zhan, T. *et al.* Transfer matrix method for optics in graphene layers. *J. Phys. Condens. Matter* **25**, 215301 (2013).
34. Walls, D. & Milburn, G. J. *Quantum Optics* Vol. 2 (Springer, Berlin, 2008).
35. Peng, Q. W. H. *et al.* Generation of two-mode quadrature-phase squeezing and intensity-difference squeezing from a cw-nopo. *Appl. Phys. B* **66**, 755–758 (1998).
36. Fabre, H. E. J. C. G. M. C. & Giacobino, E. Cavity qed effects in semiconductor microcavities. *J. Opt. B Quant. Semiclass. Opt.* **1**, 215301 (1999).
37. Fabre, C. *et al.* Quantum-noise reduction using a cavity with a movable mirror. *Phys. Rev. A* **49**, 1337–1343 (1994).

38. Qasymeh, M. Phase-matched coupling and frequency conversion of terahertz waves in a nonlinear graphene waveguide. *J. Lightw. Technol.* **35**, 1654–1662 (2017).
39. Girvin, A. B. S. & Oliver, W. Quantum information processing and quantum optics with circuit quantum electrodynamics. *Nat. Phys.* **16**, 247–256 (2020).

Acknowledgements
This research is supported by the Abu Dhabi award for research excellence Grant (AARE19-062) 2019.

Author contributions
M.Q. conceived the idea, developed the numerical model, prepared the presented results, and took the lead in writing the manuscript. H.E. contributed to the developed model, validated the obtained results, and contributed to the manuscript writing.

Competing interests
The authors declare no competing interests.

Additional information
Supplementary information is available for this paper at https://doi.org/10.1038/s41598-020-73363-y.

Correspondence and requests for materials should be addressed to M.Q.

Reprints and permissions information is available at www.nature.com/reprints.

Publisher's note Springer Nature remains neutral with regard to jurisdictional claims in published maps and institutional affiliations.